European Journal of Cell Biology 103 (2024) 151411

Contents lists available at ScienceDirect

European Journal of Cell Biology

journal homepage: www.elsevier.com/locate/ejcb

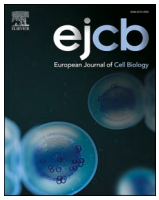

Short communication

Degradation of hexosylceramides is required for timely corpse clearance via formation of cargo-containing phagolysosomal vesicles

Rebecca Holzapfel [a], Agata Prell [b], Fabian Schumacher [b,c], Veronika Perschin [a], José Pedro Friedmann Angeli [d], Burkhard Kleuser [b], Christian Stigloher [a], Gholamreza Fazeli [d,*]

[a] Imaging Core Facility, Biocenter, University of Würzburg, Würzburg, Germany
[b] Institute of Pharmacy, Freie Universität Berlin, Berlin, Germany
[c] Core-Facility BioSupraMol, Pharma-MS subunit, Freie Universität Berlin, Germany
[d] Chair of Translational Cell Biology, Rudolf Virchow Center for Integrative and Translational Bioimaging, University of Würzburg, Würzburg, Germany

ARTICLE INFO

Keywords:
Phagolysosome resolution
Cell corpse clearance
Lysosome
Sphingolipidome
Hexosylceramides
Glucosyl ceramidases
Polar body

ABSTRACT

Efficient degradation of phagocytic cargo in lysosomes is crucial to maintain cellular homeostasis and defending cells against pathogens. However, the mechanisms underlying the degradation and recycling of macromolecular cargo within the phagolysosome remain incompletely understood. We previously reported that the phagolysosome containing the corpse of the polar body in *C. elegans* tubulates into small vesicles to facilitate corpse clearance, a process that requires cargo protein degradation and amino acid export. Here we show that degradation of hexosylceramides by the prosaposin ortholog SPP-10 and glucosylceramidases is required for timely corpse clearance. We observed accumulation of membranous structures inside endolysosomes of *spp-10*-deficient worms, which are likely caused by increased hexosylceramide species. *spp-10* deficiency also caused alteration of additional sphingolipid subclasses, like dihydroceramides, 2-OH-ceramides, and dihydrosphingomyelins. While corpse engulfment, initial breakdown of corpse membrane inside the phagolysosome and lumen acidification proceeded normally in *spp-10*-deficient worms, formation of the cargo-containing vesicles from the corpse phagolysosome was reduced, resulting in delayed cargo degradation and phagolysosome resolution. Thus, by combining ultrastructural studies and sphingolipidomic analysis with observing single phagolysosomes over time, we identified a role of prosaposin/SPP-10 in maintaining phagolysosomal structure, which promotes efficient resolution of phagocytic cargos.

1. Introduction

Maintaining cellular homeostasis heavily depends on proper vesicle trafficking to lysosomes and subsequent cargo degradation. Lysosomal degradation is responsible for recycling nutrients and safeguarding cells against harmful cargo. Phagocytosis is an essential component of the innate immune response to pathogens playing a central role in tissue homeostasis by clearing cell corpses and debris. Extensive research has revealed mechanisms of phagosome formation, maturation and fusion with lysosomes, but the final stage, where a phagolysosome resolves, degrading the cargo and recycling of its macromolecules, remains elusive. This lack of understanding stems from previous challenges in accurately monitoring individual phagolysosomes over extended periods, particularly due to the widespread use of non-degradable inorganic beads as phagocytic cargos.

By tracking a single cell corpse in early *C. elegans* embryos, we showed the stereotypical engulfment of the second polar body by large embryonic cells (Fazeli et al., 2018). After fusion with lysosomes and initial corpse membrane breakdown, phagolysosomes tubulate to form small cargo-containing vesicles to facilitate the degradation of cargo. Accordingly, inhibiting phagolysosomal vesiculation delayed cargo degradation and phagolysosomal resolution (Fazeli et al., 2018), supporting a central role for delivery of cargo into phagolysosomal vesicles in cargo degradation. Cathepsin L (CPL-1)-mediated degradation of cargo proteins is required for corpse clearance (Xu et al., 2014) and more intriguingly, transport of amino acids out of lysosomes by the solute carrier/transporter SLC-36.1 is required for ARL-8-mediated tubulation and vesiculation of the polar body phagolysosome (Fazeli et al., 2023b). These findings reveal that the initial products of degradation of cargo proteins contribute to the final resolution of the phagolysosome.

* Corresponding author.
E-mail address: gholamreza.fazeli@uni-wuerzburg.de (G. Fazeli).

https://doi.org/10.1016/j.ejcb.2024.151411
Received 24 August 2023; Received in revised form 3 April 2024; Accepted 4 April 2024
Available online 5 April 2024

However, the corpse membrane needs to breakdown first to allow lysosomal hydrolases to degrade corpse protein content. In addition to the corpse plasma membrane, other cellular lipids are also degraded inside phagolysosome. Whether deficiency in degrading cargo lipids could interfere with phagolysosome resolution is less clear. Deficiency in degrading the autophagosomal inner membrane in phospholipase A2 group XV PLA2G15/*plag-15* mutant worms and cultured mammalian cells led to the formation of persisting enlarged autolysosomes (Li et al., 2022). Since lipid membranes constitute a considerable fraction of engulfed corpse, it is plausible that deficient degradation of lipids inside corpse phagolysosome would also interfere with phagolysosome resolution.

Sphingolipids are an abundant and diverse group of membrane lipids that play structural and functional roles in cells. Unlike in mammals, sphingolipids in *C. elegans* are based on an unusual *iso*-d17:1 or *iso*-d17:0 branched-chain sphingoid base (Chitwood et al., 1995). Besides common fatty acids, *C. elegans* also attaches 2-hydroxy (2-OH)-modified fatty acids to the sphingoid moiety *via* amide bonding. Especially in glycoceramides, 2-OH fatty acids with chain lengths between C20 and C26 are attached to the sphingoid backbone (Hanel et al., 2019; Scholz et al., 2021). Glycosphingolipids and sphingomyelin are hydrolyzed in lysosomes to produce ceramides and sphingosine, which are then transported out of lysosomes for recycling or signaling purposes (Shayman, 2000). For hydrolysis of glycosphingolipids, small non-enzymatic lysosomal proteins called saposins are required, which are formed from cleavage of a single precursor Prosaposin/PSAP (Henseler et al., 1996). The four saposins yielded from PSAP cleavage are essential to mediate the interaction between membrane bound lipids and water-soluble lysosomal exohydrolases at low lysosomal pH and show a rather broad specificity for sphingolipid species. Mutations in the PSAP gene are associated with lysosomal storage diseases, including Gaucher disease, and metachromatic leukodystrophy (Morimoto et al., 1990). Whether prosaposin deficiency also affects phagolysosomal clearance is unclear.

Here, we report that phagolysosome degradation of cargo lipids and proteins is impaired in Prosaposin/*spp-10*-deficient worms. We have found that this impaired degradation is, at least in part, due to a reduction in the formation of the cargo-containing vesicles from phagolysosomes. However, decreased vesiculation of the phagolysosome is not attributed to mislocalization of ARL-8 from the lysosomes, a protein crucial for membrane tubulation. Thus, using an *in vivo* model to observe resolution of a single phagolysosome, we revealed that PSAP/SPP-10 is required for maintaining phagolysosomal dynamics to resolve phagocytic cargos.

2. Materials and methods

2.1. Worm strains and maintenance

C. elegans strains were grown at room temperature according to standard procedures (Brenner, 1974). *C. elegans* strains used are detailed in Table S1 (Beer et al., 2018; Consortium 2012; Gan et al., 2019; Njume et al., 2022). Worms were PCR genotyped for the *spp-10(ok1585)* deletion using the following primers: spp-10_Ex1_For (CGT TCT CGG CTC AAC TCT TGC), spp-10_Int7_Rev (GGT GGC ATA CTT GAC AGC TGC), and spp-10_Ex3_Rev (CAC AGA CGA TGG CTG GCT TAA C).

2.2. RNAi experiments

RNAi-mediated knockdown was performed by feeding dsRNA-expressing bacteria at 22–25°C from the L1 larval stage through adulthood (62–72 hours) according to established protocols (Fraser et al., 2000). RNAi constructs were obtained from available libraries (Source BioScience, *gba-1* (mv_C33C12.3), *gba-2* (mv_C33C12.8), *gba-3* (mv_F11E6.1), *gba-4* (mv_Y4C6B.6), *sam-4* (sjj_F59E12.11), *spp-8* (mv_C28C12.5), and *spp-10* (sjj_C28C12.7)).

2.3. Light microscopy

Embryos dissected on a cover slip in M9 buffer were mounted on a slide on top of an agarose pad for time lapse analysis, as described previously (Fazeli et al., 2023a). Sixteen 1.2 μm step Z-stacks were acquired sequentially for mCherry and DIC or mCherry and GFP every minute at room temperature using a DM5500 wide-field fluorescence microscope with a HC PL APO 40×1.3 NA oil objective lens supplemented with a DFC365 FX CCD camera controlled by LAS AF software (Leica). Confocal images were obtained using a Leica SP2 confocal with a HCX PL APO CS 40×1.25 NA oil objective with photomultiplier detectors.

2.4. Antibody staining

Gravid worms were dissected in water on a coverslip to release embryos and transferred to 0.1% polylysine-coated slides and frozen on dry ice. Eggshells were cracked by flicking off the coverslip and embryos were fixed in methanol before staining with chicken α-GFP (Aves) and rabbit α-DsRed (Takara) antibodies (1:200). Slides were counterstained with DAPI to label DNA and mounted using DABCO.

2.5. Image analysis

Time-lapse series were analyzed using Imaris (Oxford Instruments). Internalization was defined as the first frame where the polar body moves away from the plasma membrane, which is likely to closely reflect closure of the phagocytic cup (Fazeli et al., 2018). Vesiculation events were scored when the vesicles were clearly distinct from each other, likely underestimating budding events. Each vesicle was followed individually until disappearance. Degradation was defined as the last frame where mCh reporters were observed after examining the following three frames for mCh puncta reappearance. Acidification was defined as the last frame where EGFP reporters were observed after examining the following three frames for EGFP puncta reappearance.

2.6. Fluorescence intensity measurements

To assess initial acidification of the phagolysosomal lumen, mean fluorescence intensity for GFP::- and mCh::Histone H2B was measured in both channels in the same 3 μm^2 circle around the 2nd polar body using Fiji (Schindelin et al., 2012). Fluorescence intensity was measured from 5 minutes before engulfment until GFP marker visually disappeared from the polar body phagolysosome. Fluorescence intensity in cytoplasm at 5 time points with 10 min intervals was measured and averaged for background subtraction. The ratio of GFP to mCh fluorescence is reported in percent.

2.7. Image processing

For clarity, images were rotated, colorized and the intensity was adjusted using Adobe Photoshop. All images show a single optical section (Z), except for Fig. 4A-E, where maximum projection of two to four Zs with 1.2 μm steps are shown.

2.8. Transmission electron microscopy (TEM) and quantification of TEM images

For TEM analysis, worms were immobilized by high pressure freezing, followed by freeze substitution and embedded in Epon as described in detail previously (Link et al., 2018). ~70 nm thin sections were then examined under a JEOL JEM-2100 TEM operated at 200 kV acceleration voltage. EM micrographs were recorded with a TemCam F416 4k×4k camera (Tietz Video and Imaging Processing Systems). Endolysosomes in hypodermis of adult worms (Figs. 1 and 3) or in embryos (Figure S1) were analyzed.

For unbiased quantification of TEM images, 25 images per experimental condition were randomly selected using a number generator and blinded. The blinded images were mixed, and all images were analyzed together, regardless of the experimental condition. The morphology or size of the structures of interest was determined using Fiji (Schindelin et al., 2012), before unblinding.

2.9. Sample preparation for sphingolipidome analysis

Worm strains were synchronized by bleaching to exclude the age variability in samples. The embryos were then transferred to NGM lite plates with *E. coli* HT115 bacteria expressing vector, *gba-2*, *gba-3*, or *spp-10* RNAi. After 65–72 h worms were collected, washed several times in M9 and pelleted by centrifugation. The worm pellet was then frozen in liquid nitrogen and stored at −80°C until further analysis.

2.10. Quantification of C. elegans-specific sphingolipids by HPLC-MS/MS

Worm pellets were homogenized in aqueous buffered solution using a Beadruptor 12 (Omni International), and then the protein content of the lysate was determined using Bradford assay. Volumes corresponding to a protein content of 0.5–2 mg were subjected to lipid extraction using 1.5 mL methanol/chloroform (2:1, v:v) containing 17:0 ceramide (Cer d18:1/17:0) and d_{31}-16:0 sphingomyelin (SM d18:1/16:0-d_{31}) (both Avanti Polar Lipids) as internal standards. Extraction was facilitated by incubation at 48°C with gentle shaking overnight. To reduce interference from glycerolipids, samples were saponified with 150 µL of 1 M methanolic KOH for 2 h at 37°C with gentle shaking followed by neutralization with 12 µL glacial acetic acid. After centrifugation at 2200 g for 5 min, organic supernatants were evaporated to dryness using a Savant SpeedVac concentrator (Thermo Fisher Scientific). Dried samples were prepared for analysis through reconstitution in 100 µL acetonitrile/methanol/water (47.5:47.5:5 (v:v:v), 0.1% formic acid). Chromatographic separation was achieved on a 1290 Infinity II HPLC (Agilent Technologies) equipped with a Poroshell 120 EC-C8 column (3.0×150 mm, 2.7 µm; Agilent Technologies) guarded by a pre-column (3.0×5 mm, 2.7 µm) of identical material. A mobile phase system consisting of water (eluent A) and acetonitrile/methanol (1:1, v-v; eluent B), both acidified with 0.1% formic acid, was used for gradient elution at an initial composition of 40:60 (A:B, v-v) and a flow rate of 0.5 mL/min (Table S2). We first followed a non-targeted approach to identify the sphingolipid species that could be detected with our protocol, with reference to a recent publication (Scholz et al., 2021). Using a high-resolution 6550 quadrupole time-of-flight mass spectrometer (Agilent Technologies), we detected all 45 species identified in the abovementioned study in our preparations with a mass error of less than 3 ppm (data not shown). From this panel, we selected 35 sphingolipid species for targeted LC-MS/MS quantification applying the multiple reaction monitoring (MRM) approach (Table S3). MRM analyzes were carried out using a 6495 triple-quadrupole mass spectrometer (Agilent Technologies) operating in the positive electrospray ionization mode (ESI+). The following ion source parameters were set: sheath gas temperature, 375 °C; sheath gas flow, 12 L/min of nitrogen; nebulizer pressure, 20 psi; drying gas temperature, 240 °C; drying gas flow, 20 L/min of nitrogen; capillary voltage, 4000 V; nozzle voltage, 2000 V; iFunnel high pressure RF voltage, 90 V and iFunnel low pressure RF voltage, 60 V. Peak areas of dhCer, Cer, 2-OH-Cer, dhSM, SM and 2-OH-SM subspecies were normalized to those of their corresponding internal standards followed by external calibration in the range of 1 fmol to 50 pmol on column using mammalian-like sphingolipid reference standards (Table S3). Due to lack of a proper calibration reference compound, 2-OH-HexCer were determined semi-quantitatively by normalizing their peak areas using those of the most abundant sphingolipid in the lipid extract, SM t39:1 (constantly approx. 40 mol%, see also Fig. S2). Data evaluation was performed with MassHunter software (Qualitative Analysis 10.0 and Quantitative Analysis 10.1, both Agilent Technologies).

2.11. Quantification and statistical analysis

Student's one-tailed t-test (Microsoft Excel), two-way ANOVA, or Chi-squared test (Graph Pad Prism) were used to test statistical significance using the Bonferroni correction to adjust for multiple comparisons. Each circle in graphs represents one organelle (Fig. 1E) or one phagolysosome of an embryo (Fig. 4N-O). Therefore, the number of circles denotes the n in each experiment. Mean ± standard error of the mean is depicted in graphs and stated in the text, except for Fig. 2 A-B and 3 F-G, where mean ± standard deviation is shown.

3. Results

3.1. The prosaposin SPP-10 is required for lipid degradation in endolysosomes

C. elegans has several proteins with saposin-like domains, including SPP-7, SPP-8, SPP-10 and two shorter proteins SPP-13, and SPP-15. Among these SPP-8 and SPP-10 are recognized as orthologs of mammalian PSAP using database search (Alliance of Genome Resources, 2022). SPP-10 also shows homology to mammalian PSAPL1 and SFTPB and is the only of the *C. elegans* prosaposin-like proteins with considerable expression during the time of polar body corpse clearance (Tintori et al., 2020). We first asked whether SPP-10 is required for maintaining endolysosomal morphology. We analyzed the ultrastructure of worms using transmission electron microscopy mainly in hypodermis, a tissue with considerable phagocytosis activity (Wang et al., 2023) and well described lysosomal morphology (Li et al., 2016; Sun et al., 2020). We examined young adult wildtype animals or worms deficient for *spp-10* by RNAi-mediated knockdown (covering the first five exons) or harboring a deletion mutation (*ok1585,* which lacks the first six exons). We discovered that *spp-10* deficiency by RNAi or in mutants leads to development of electron-dense organelles containing multilayered membranes and intraluminal vesicles (Fig. 1A-E). These structures probably indicate lipid accumulation in defective endolysosomes. We did not observe an additional increase in the number or area of the defective endolysosomes in the deletion mutants after treatment with *spp-10* RNAi (Fig. 1D-E), denoting that there are no additional off-target effects of the RNAi. We also noticed fused endolysosomes in *spp-10*-knockdown embryos (Fig. S1), which may be the early stages of the complex organelles in Fig. 1B-D. These data reveal that SPP-10 plays a critical role in maintaining endolysosomal dynamics and functions in embryos and adult worms, similar to the role of PSAP in mammals (Meyer et al., 2014).

3.2. Loss of SPP-10 causes accumulation of sphingolipid subspecies

As mammalian PSAP is required for degradation of several sphingolipid species (Rorman et al., 1992), we next asked which sphingolipids are regulated by SPP-10. To check the levels of different sphingolipid subclasses, we measured a total of 35 sphingolipid species from the groups of dihydroceramides (dhCer), ceramides (Cer), 2-OH-ceramides (2-OH-Cer), 2-OH-hexosylceramides (2-OH-HexCer), dihydrosphingomyelins (dhSM), sphingomyelins (SM), and 2-OH-sphingomyelins (2-OH-SM) in whole animal extracts by liquid chromatography coupled with tandem-mass spectrometry (HPLC-MS/MS). While levels of Cer, SM and 2-OH-SM were unaffected by *spp-10* knockdown or deletion, we observed elevated levels of dhCer, 2-OH-Cer and dhSM in these worms (Fig. 2A). Intriguingly, dhCer were increased in both RNAi-mediated knockdown and *spp-10(ok1585)* mutants with dhCer d38:0 and dhCer d41:0 showing the strongest effect of >60% increase over controls (Fig. 2C). As mammalian PSAP is required for degradation of glycosphingolipids (Rorman et al., 1992), we were particularly interested in the amounts of hexosylceramides. Consistent

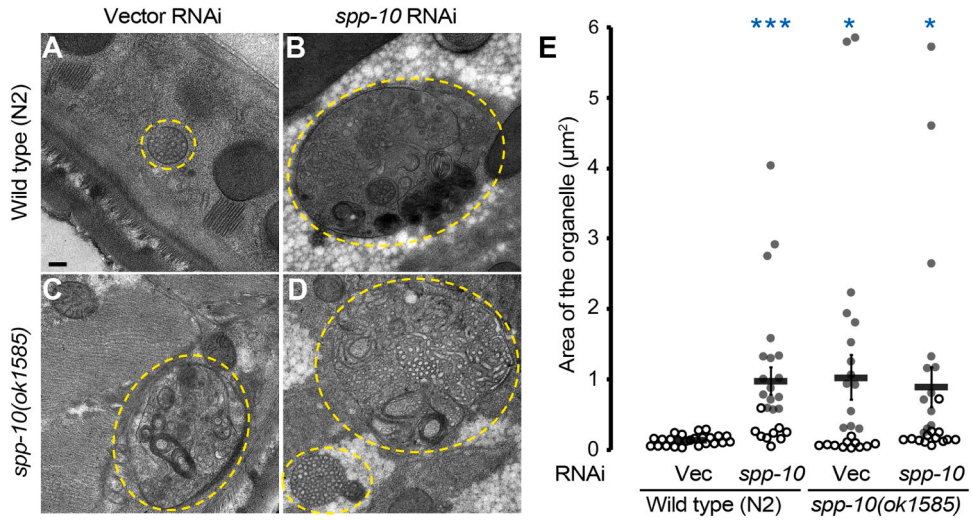

Fig. 1. SPP-10 is required to maintain the morphology of endolysosomes A-D) Transmission electron micrographs showing endolysosomes (dark multi-vesicular bodies (MVB) or lysosomes) in hypodermis of control N2 strains or *spp-10(ok1585)* deletion mutants after treatment with vector or *spp-10* RNAi. Yellow dashed ovals show the approximate boundaries of the organelles. Scale bar is 200 nm. E) Quantification of the area of endolysosomes. Each circle denotes one organelle. Open circles denote organelles with normal morphology of MVB or lysosomes. Closed circles denote abnormal morphology with accumulation of MVB, multi-layered membranous organelles and other structures all inside a single limiting membrane. Mean ± SEM is shown. *p<0.05, ***p<0.001 compared to control embryos using Student's t-test with Bonferroni correction.

with a recent study, we only analyzed hexosylceramides N-acylated with a 2-OH-modified fatty acid (Hanel et al., 2019; Scholz et al., 2021). As predicted, we noticed that 2-OH-HexCer species also accumulated in *spp-10*-deficient worms (Fig. 2B, D). HexCer t39:1 bearing a 2-hydroxylated 22:0 fatty acid side-chain, was the most abundant 2-OH-HexCer species detected (see Fig. S2 for a representative HPLC-MS/MS chromatogram), followed by HexCer t41:1 which is in accordance to literature data as recently reviewed (Xatse and Olsen, 2023). These quantitative data identify dhCer and 2-OH-HexCer as likely contributors to abnormal morphology of the endolysosomes in *spp-10*-deficient worms.

3.3. Loss of individual glucosylceramidases show similar but weaker phenotypes to spp-10 mutant worms

We next asked whether the changes in the morphology of endolysosomes and accumulation of sphingolipid species can be phenocopied by knocking down glucosylceramidases. *C. elegans* has four putative glucosylceramidases GBA-1 to -4, the enzymes that degrade glucosylceramides in low lysosomal pH and need saposin C for activation (Weiler et al., 1995). Our TEM analysis showed a mild accumulation of electron dense structures inside endolysosomes after RNAi-mediated knockdown of *gba-2, gba-3* and to a smaller extent *gba-4*, whereas knocking down *gba-1* did not affect the morphology of the endolysosomes (Fig. 3A-E). These results demonstrate that loss of the ability to breakdown glucosylceramides leads to accumulation of lipids inside endolysosomes, similar to what we observed in *spp-10* -deficient worms. As *spp*-10-deficient worms showed a more pronounced phenotype, these data also indicate that SPP-10 may be required for the activity of several of the glucosylceramidases or other enzymes in *C. elegans*, which might act redundantly to each other.

To confirm that the lipid accumulation inside endolysosomes of *gba-2* and *gba-3* worms is caused by the accumulation of hexosylceramides, we quantified the sphingolipidome of these worms. We observed an increase in total levels of 2-OH-HexCer species in the *gba-2* and even further in *gba-3* worms (Fig. 3G, I). Further, while SM, dhSM and 2-OH-Cer were not affected after *gba-2* and *gba-3* knockdown, levels of Cer and dhCer increased only after *gba-2* knockdown and 2-OH-SM were decreased after *gba-2* and *gba-3* knockdown (Fig. 3F-H). Altogether, our results confirm a central role of the 2-OH-HexCer accumulation on the abnormal morphology of endolysosomes in *gba-2-, gba-3-*, and *spp-10*-deficient worms, whereas single deficiency in *gba-1* and *gba-4* does not seem to affect endolysosomes dramatically.

3.4. SPP-10 is required for vesiculation and timely resolution of cell corpses

To determine whether accumulation of hexosylceramides would interfere with lysosomal functions we tested whether preventing degradation of these sphingolipids would lead to formation of persisting cell corpses in *C. elegans* embryos. Control embryos typically clear the corpse of the second polar body by the 88-cell stage (Fazeli et al., 2018). Therefore, we first depleted SPP-10 or SPP-8, two of the *C. elegans* PSAP orthologs and analyzed whether we observe a persisting polar body corpse around 88-cell stage. We found an increased number of embryos with a persisting polar body corpse (Fig. 4A-C & F, by 7-fold in *spp-10* RNAi, 90%, n=20 vs. 12%, n=25 in controls and by 4-fold in *spp-8* RNAi, 52%, n=25). To ensure that persisting corpse phenotype in *spp*-deficient embryos is caused by accumulation of glucosylceramides including hexosylceramides, we examined corpse clearance after knocking down glucosylceramidases. Knocking down GBA-2, GBA-3, and GBA-4 caused elevated number of embryos with persisting corpse (Fig. 4D-F, by 6-fold in *gba-2* RNAi, 70%, n=23, by 6-fold in *gba-3* RNAi, 70%, n=20, and by 4-fold in *gba-4* RNAi, 52%, n=21), whereas GBA-1 knockdown embryos were not different from controls (Fig. 4F, 10%, n=20). Altogether, these results demonstrate that deficient degradation of hexosylceramides including glucosylceramides in embryos lacking PSAP proteins or saposin-dependent glucosylceramidases lead to defective corpse clearance.

Next, we confirmed that degradation of phagolysosomes is defective in *spp-10* knockdown worms using time-lapse imaging. For this purpose we used an *mCherry::PH::ZF1* tag to label the protein cargo inside corpse phagolysosome. With pKa of 4.5, mCherry fluorescence fused to proteins is stable in the acidic environment of lysosomes (Green et al., 2008). Therefore, we considered mCherry disappearance as an approximation of protein degradation inside phagolysosomes. The corpse phagolysosome disappeared ~90 min after engulfment in controls but persisted for >150 min past engulfment after *spp-10* knockdown (Fig. 4G-H, J-K, O). To ensure the specificity of our RNAi knockdown, we examined corpse degradation in *spp-10(ok1585)* deletion mutants and found a

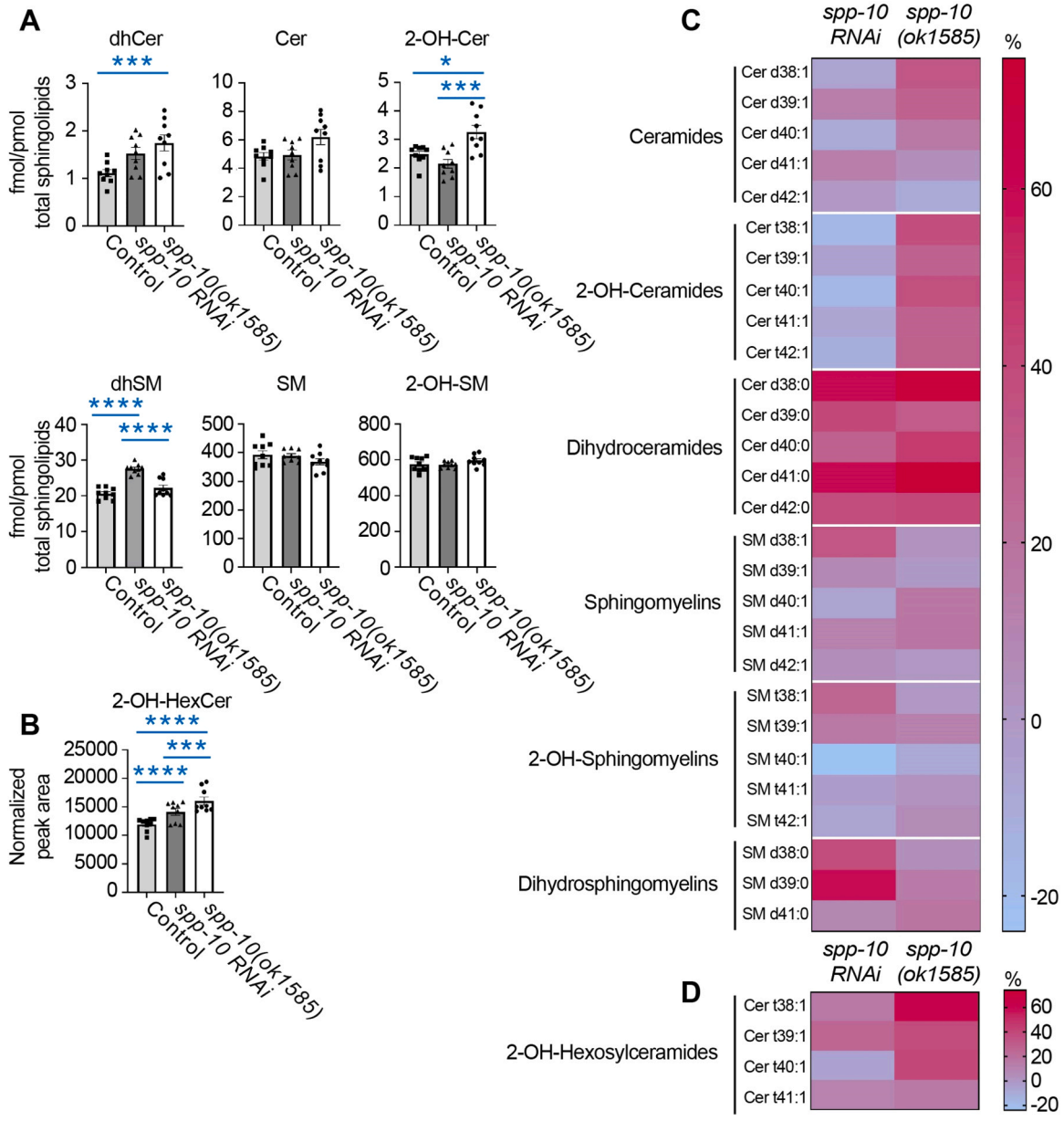

Fig. 2. Loss of SPP-10 causes accumulation of sphingolipid subspecies A-B) Lipidomic analysis of dihydroceramides (dhCer), ceramides (Cer), 2-OH-ceramides (2-OH-Cer), dihydrosphingomyelins (dhSM), sphingomyelins (SM), and 2-OH-sphingomyelins (2-OH-SM) (A), as well as 2-OH-hexosylceramides (2-OH-HexCer) (B) from vector or *spp-10* RNAi-treated, or *spp-10(ok1585)* mutant worms. Bars show mean ± SD. Single measurements are shown as dots. *p<0.05, ***p<0.001, ****p<0.0001 using 2-way ANOVA corrected for multiple comparisons. C-D) Heat map analysis of the indicated sphingolipid species with different chain length. % changes compared to controls are depicted. Not shown chain lengths were below detection limits. Heat maps are generated from average of three technical repeats of three independent biological samples (3×3 measurement points).

similar >150 min delayed corpse content degradation (Fig. 4I, L, O). These data reveal that SPP-10 is necessary for timely phagolysosome resolution.

We then asked whether corpse persistence was caused by defective engulfment or degradation. Time-lapse imaging analysis revealed that the corpse of the polar body was engulfed with normal timing after *spp-10* knockdown (5±1 min after 4-cell stage, n=11 vs. 2±1 min, n=10 in controls, p= 0.12) or in *spp-10(ok1585)* mutants (6±2 min, n=8 after 4-cell stage, slightly longer than controls, p=0.02, Fig. 4J-L), indicating that corpse engulfment does not require SPP-10.

We next asked whether lysosome-mediated corpse membrane breakdown (CMBD) is affected in *spp-10*-deficient worms. CMBD is the first step of membrane degradation to give lysosomal hydrolases access to corpse inner cargo (Fazeli et al., 2018). CMBD occurred with similar timing in vector- or *spp-10*-treated RNAi (9±1 min after 4-cell stage, n=11 vs. 11±1 min, n=10 in controls, p=0.29) or in *spp-10(ok1585)* mutants (14±1 min after 4-cell stage, n=8, p=0.07 vs. controls, Fig. 4J-L). To verify that lysosomal fusion with corpse phagosome is not affected in *spp-10*-deficient worms, we tested the initial acidification of lysosomal lumen in vector- or *spp-10*-treated RNAi embryos using the intrinsic pH sensitivity of an EGFP marker. EGFP has a pKa of 6.0 and quickly quenches in the acidic environment of the lysosome (Green et al., 2008). Therefore, we used a *GFP::ZF1::PH(PLC1delta1)* marker to label the corpse phagolysosome, which would quench after fusion with lysosomes. The GFP marker disappeared from vector- or *spp-10*-treated RNAi embryos with similar timing (21 ± 2 min after engulfment in vector (n=13) vs. 27 ± 3 in *spp-10*-deficient embryos (n=10), p=0.06). To confirm these results, we measured the fluorescence intensity of GFP

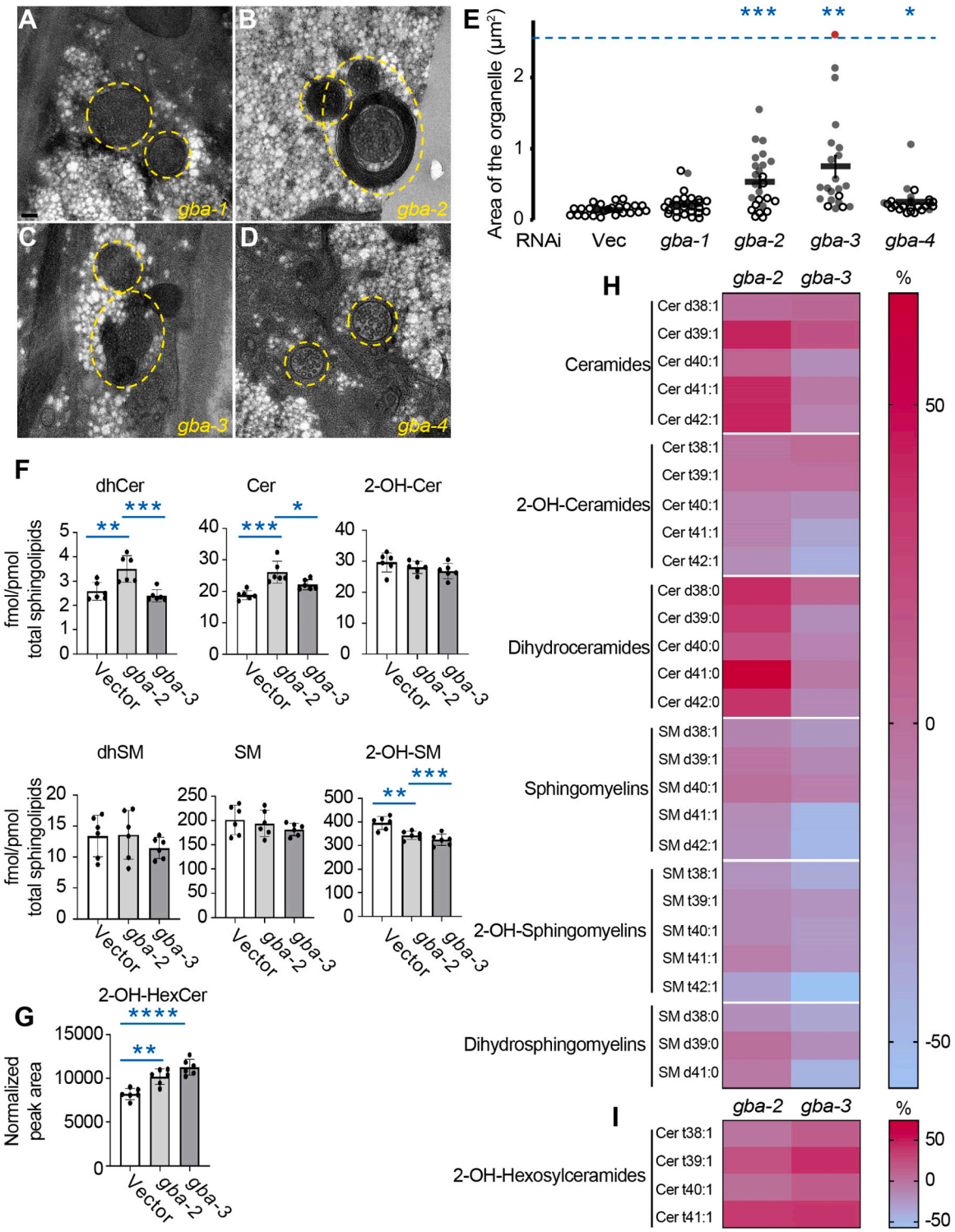

Fig. 3. Loss of individual glucosylceramidases show similar but weaker phenotypes to *spp-10* mutant worms. A-D) Transmission electron micrographs showing endolysosomes in hypodermis of worms treated with RNAi against *gba-1* (A), *gba-2* (B), *gba-3* (C), or *gba-4* (D). Yellow dashed ovals show the approximate boundaries of the organelles. Scale bar is 200 nm. E) Quantification of the area of endolysosomes. Each circle denotes one organelle. Open circles denote organelles with normal morphology of MVB or lysosomes. Closed circles denote abnormal morphology with accumulation of MVB, multi-layered membranous organelles and other structures all inside a single limiting membrane. The red circle above the blue dashed line denotes an outlier with an area of 4.4 square micrometer. Mean ± SEM is shown. *p<0.05, **p<0.01, ***p<0.001 compared to control embryos using Student's t-test with Bonferroni correction. F-G) Lipidomic analysis of dihydroceramides (dhCer), ceramides (Cer), 2-OH-ceramides (2-OH-Cer), dihydrosphingomyelins (dhSM), sphingomyelins (SM), and 2-OH-sphingomyelins (2-OH-SM) (F), as well as 2-OH-hexosylceramides (2-OH-HexCer) (G) from vector, *gba-2* or *gba-3* RNAi-treated worms. Bars show mean ± SD. Single measurements are shown as dots. *p<0.05, **p<0.01, ***p<0.001, ****p<0.0001 using 2-way ANOVA corrected for multiple comparisons. H-I) Heat map analysis of the indicated sphingolipid species with different chain length. % changes compared to controls are depicted. Not shown chain lengths were below detection limits. Heat maps are generated from average of two technical repeats of three independent biological samples (3×2 measurement points).

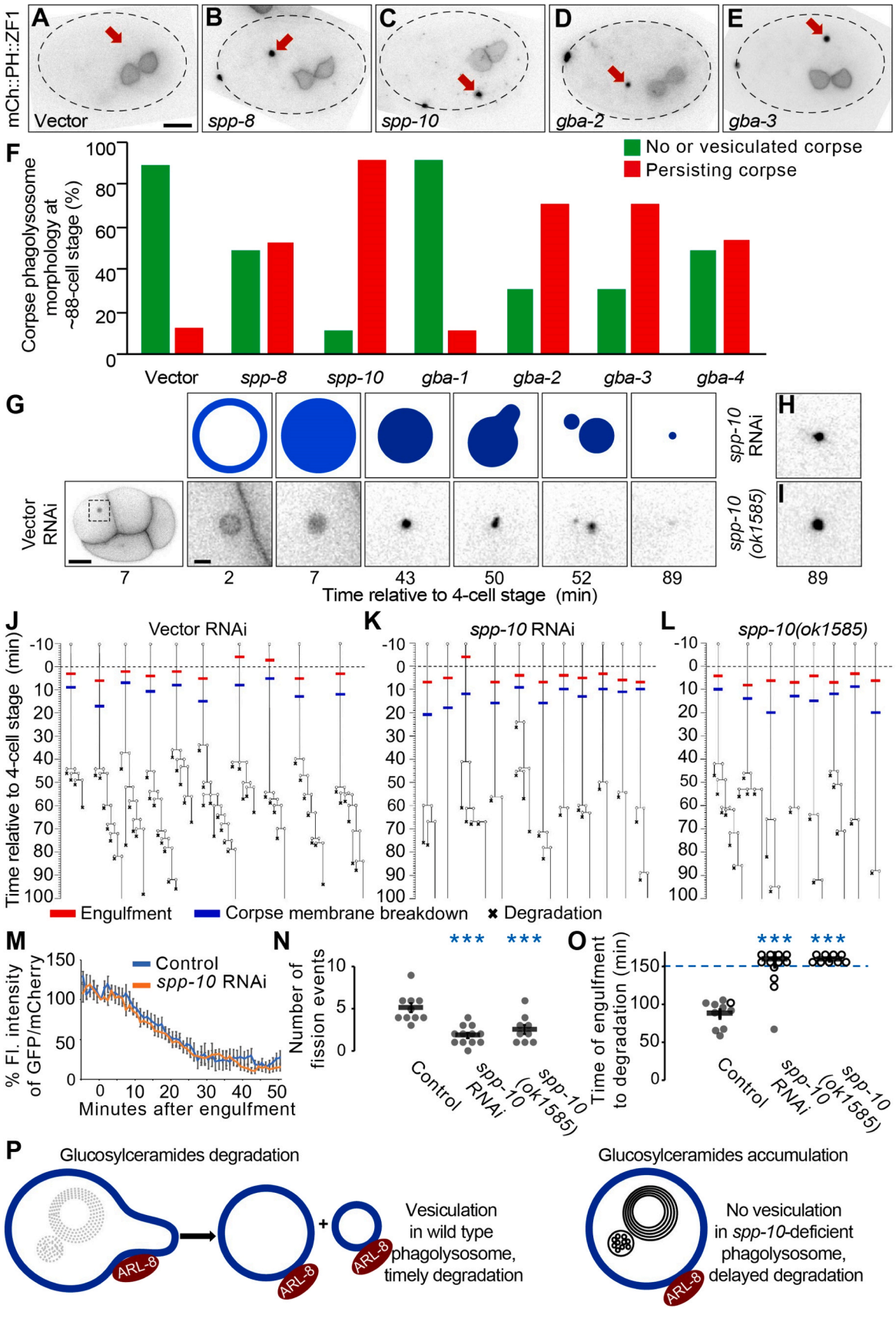

(caption on next page)

Fig. 4. SPP-10 is not required for corpse phagocytosis and corpse membrane breakdown, but is needed for phagolysosome resolution and cargo degradation A-E) Images of embryos expressing mCh::PH::ZF1 at around the 88-cell stage after treatment with vector (A), *spp-8* (B), *spp-10* (C) , *gba-2* (D), or *gba-3* (E) RNAi. The polar body corpse or its remains are marked with an arrow. Dashed line indicates the approximate boundaries of the embryo. The two germ cells (grey) are used as a guide to spot the 88-cell stage. Scale bar is 10 μm. F) Quantification of morphology of the polar body corpse phagolysosomes in embryos treated with vector (n=25), *spp-8* (n=25), *spp-10* (n=20), *gba-1* (n=20), *gba-2* (n=23), *gba-3* (n=20), or *gba-4* (n=21) RNAi. Embryos around the 88-cell stage (~90 min past engulfment) are analyzed. G) Representative images from a time-lapse series showing the fate of the second polar body corpse in a control embryo. The upper panels show schematic representation of the corpse. Numbers indicate minutes after 4-cell stage. After engulfment (2, red rectangle in J) the corpse membrane breaks down inside the phagolysosome, indicated by dispersion of the membrane tag inside the lumen (7, blue rectangle in J). The phagolysosome gradually shrinks (43) and next tubules containing cargo are formed (50), which then are released as small vesicles (52, branches in J) before degradation (shortly after 89, X in J). Typically, ~5 rounds of vesiculation occur before the tagged cargo disappears. Scale bars in the main panel and magnified inset show 10 and 2 μm respectively. H-I) After *spp-10* knockdown (H) or in *spp-10(ok1585)* deletion mutants (I) fewer fission events occur, delaying degradation of corpse phagolysosome. J-L) Tracing cargo-containing phagolysosomal vesicles (new branch point) from vector or *spp-10* RNAi-treated, or *spp-10(ok1585)* mutant embryos. The phagolysosome tubulates into vesicles, which disappear (X) within few minutes of their birth to facilitate degradation of the main phagolysosome (X). After *spp-10* knockdown or in *spp-10(ok1085)* mutants, fewer fission events occur. The lineage is not marked with an X if the polar body phagolysosome persisted for >100 min past the 4-cell stage. See O for the time of disappearance. Each vertical line represents one corpse phagolysosome. Rectangles represent timing of polar body engulfment (red) or corpse membrane breakdown (blue). M) The ratio of fluorescence intensity of the corpse phagosome cargo GFP::H2B to mCherry::H2B as an approximation of the time of initial lumen acidification in control (blue, n=10) or *spp-10* RNAi-treated embryos (orange, n=10). N) Phagolysosomal fission events were reduced compared to control embryos (5±1) in *spp-10* knockdown (2±0), or *spp-10(ok1585)* (3±1) mutants. O) In control embryos, the mCherry-tagged protein cargo disappears from the phagolysosome 88±6 min after engulfment. Cargo degradation was delayed >150 min in *spp-10* knockdown or in *spp-10(ok1585)* mutants. Each circle denotes one phagolysosome. Open circles denote the last frame of a time-lapse series in which the polar body phagolysosome did not disappear. Mean ± SEM is shown. Disappearance times and means beyond 150 min after engulfment are grouped above the dashed blue line. ***$p<0.001$ compared to control embryos using Student's t-test with Bonferroni correction. P) Model of the role of SPP-10 in phagolysosome resolution. Glucosylceramides are degraded in wild type phagolysosomes. Phagolysosome tubulation mediated by ARL-8 and kinesin motors lead to the formation of the cargo-containing vesicles from the phagolysosome to facilitate final cargo clearance. In *spp-10*-deficient phagolysosomes, glucosylceramides accumulate (depicted as persisting membranous structures inside the phagolysosome). Although ARL-8 still localizes to the phagolysosome, formation of cargo-containing tubules and vesicles from the phagolysosome is decreased, which ultimately leads to delayed cargo clearance.

and mCherry fused to histone H2B as another cargo marker of the corpse phagolysosome. The intensity profile of the ratio of GFP to mCh over time did not show any difference in GFP quenching between control and *spp-10* knock down groups (Fig. 4M, Supplementary Fig. 3A-B), further confirming that the fusion of the corpse phagosome with lysosomes and the initial cargo acidification is not regulated by SPP-10. Altogether, these data indicate that SPP-10 is not required for corpse phagosome fusion with lysosomes, initial lumen acidification, and the degradation of corpse membrane.

Next, we tested whether SPP-10 is required for the formation of the cargo-containing vesicles from phagolysosomes, an essential step for phagolysosome resolution (Fazeli et al., 2018). We noticed a 2-fold decrease in the frequency of the formation of the phagolysosomal cargo-containing vesicles after *spp-10* knockdown or in *spp-10(ok1585)* deletion mutant (Fig. 4J-N), indicating that this critical step for phagolysosome resolution requires SPP-10. Therefore, these findings suggest that hydrolysis of glucosylceramides in phagolysosomes is essential for timely phagolysosome resolution via the formation of the phagolysosomal cargo-containing vesicles, similar to protein degradation and amino acid transport (Fazeli et al., 2023b; Xu et al., 2014).

3.5. SPP-10 is not required for localization of ARL-8 or SLC-36.1 to lysosomes

During phagolysosome tubulation, the small GTPase ARL-8 and its adaptor protein PLEKHM2/PKHM-2 link the phagolysosomal membrane to kinesin motors to be pulled along the microtubules and allow phagolysosomal vesiculation (Fazeli et al., 2023b, 2018). As ARL-8 needs to be localized to lysosome and phagolysosomes to promote the formation of cargo-containing vesicles (Fazeli et al., 2023b), we questioned whether SPP-10 is required for recruitment of ARL-8. For this purpose, we used embryos expressing endogenously tagged ARL-8 and lysosomal marker cystinosin/CTNS-1. ARL-8 localized to distinct endolysosomal puncta after *spp-10* RNAi treatment (n=25, Supplementary Fig. 4B, D, F), similar to vector RNAi treated embryos (n=25, Supplementary Fig. 4 A, D, E), whereas, treatment with RNAi against ARL-8 putative GEF, SAM-4/myrlysin, dispersed ARL-8 in the cytosol (n=25, Supplementary Fig. 4C-D) or to the enlarged organelles, which we previously have shown to retain early endosome identity (Fazeli et al., 2023b). As the amino acid transporter SLC-36.1 is also required for phagolysosome vesiculation without affecting ARL-8 localization on phagolysosomes (Fazeli et al., 2023b), we asked whether SPP-10 could control the localization of SLC-36.1. We did not observe any changes in localization of SLC-36.1 puncta after knockdown of SPP-10 (n=7) compared to controls (n=11, Supplementary Fig. 4G-H). Further, the number of puncta and their intensity were also comparable in control and *spp-10*-deficient embryos. Importantly, we occasionally detected colocalization of SLC-36.1 and the lysosomal nuclease NUC-1 in both control and *spp-10*-deficient embryos, indicating partial localization of SLC-36.1 on lysosomes independent of SPP-10. Altogether, these data suggest that the process or the product of HexCer degradation are not required for recruitment of vesiculation machinery to the phagolysosome.

4. Discussion

Using an *in vivo* model to combine ultrastructure and lipidomics with tracking a single phagolysosome, we revealed that SPP-10, GBA-2 and GBA-3 are required for the maintenance of lysosomal morphology and function by regulating levels of 2-OH-HexCer, which eventually help corpse clearance via the formation of cargo-containing phagolysosomal vesicles (Fig. 4P). Intriguingly, a recent study in immortalized bone marrow-derived macrophages revealed that mammalian prosaposin is required for lysosomal tubulation (Barreda et al., 2024), underlining the importance of sphingolipid catabolism in lysosomal morphology and function across species.

Our quantitative data reveal that dhCer and 2-OH-HexCer are the most altered sphingolipids in *spp-10*-deficient worms, identifying likely contributors to abnormal morphology of the endolysosomes. However, our further experiments with glucosylceramidases *gba-2*- and *gba-3*-deficient worms showed a consistent elevation of 2-OH-HexCer levels in both groups, whereas compared to controls, dhCer levels were not different in *gba-3*-deficient worms, which showed a stronger phenotype of abnormal endolysosomes. Similarly, the total levels of Cer and 2-OH-SM were differently affected in *spp-10*-, *gba-2*-, and *gba-3*-deficient worms compared to controls, making the changed levels of these sphingolipid species unlikely to be the cause of the abnormal endolysosomal morphology in these mutants. Therefore, these findings support a central role of glucosylceramide removal in maintaining endolysosomal morphology and function. These data serve as a starting point for future studies to show the role of other enzymes responsible for formation, conversion or transport of these identified sphingolipids species to determine their roles in endolysosomal morphology and function.

Intriguingly, we also observed some differences between the measured levels of some sphingolipid species between knockdown and mutants, for example in 2-OH-Cer or dhSM (Fig. 2A, C). Although we did not observe any difference in TEM analysis of endolysosomes between knockdown and mutants (Fig. 1), we assume that the difference in the measured sphingolipids might reflect any residual SPP-10 protein levels after knockdown. Since dhCer and dhSM can be converted to each other, we speculate that worms still can compensate the partial loss of SPP-10 and elevated dhCer by converting a portion of them to respective dhSM species. However, in the case of complete loss of SPP-10 the animals are left with the elevated sphingolipids at the level of dhCer and not dhSM. This can affect cellular health as elevation of cytotoxic dhCer along with a decreasing Cer/dhCer ratio may trigger autophagy (Hernandez-Tiedra et al., 2016). On the other hand, increased levels of dhSM may facilitate formation of assemblies in SM-rich lipid domains, which may have significant roles in membrane-related biological processes (Kinoshita et al., 2020). Lysosomal degradation of 2-OH-HexCer would lead to *iso*-d17:1 sphingoid base via 2-OH-Cer. SPP-10 deficiency should thus lead to decreased levels of 2-OH-Cer in addition to accumulation of 2-OH-HexCer, which is at least trend-wise true for RNAi-mediated knockdown of *spp-10,* as well as *gba-2* and *gba-3*. Since 2-OH-Cer can in turn be converted to 2-OH-SM, the reduced substrate supply for sphingomyelin synthases due to 2-OH-HexCer accumulation could contribute to the reduced amounts of detected 2-OH-SM in *gba-2*- and *gba-3*-deficient worms. However, in the *spp-10* mutant, in addition to the accumulation of 2-OH-HexCer, we found significantly increased levels of its metabolite 2-OH-Cer. This could be due to increased degradation of 2-OH-SM, but we did not detect any changes in 2-OH-SM levels. One could now speculate that the mutants overcompensate for the *de novo* synthesis of 2-OH-Cer to counterbalance the losses due to inhibited catabolism of 2-OH-HexCer. Therefore, the residual activity of SPP-10 in knockdown worms or the shorter duration of RNAi treatment versus the life-long loss of the protein in deletion mutants could be among the factors why the levels of some measured sphingolipids are different in knockdown compared to stable mutants.

As SPP-10 is proposed to act in lysosomes, yet our lipidomic analysis is performed in whole animal lysate, we expect that the local increase of 2-OH-HexCer species in endolysosomes would be even more pronounced. Ideally, sphingolipid analysis should be performed on purified or enriched lysosomal fractions. This could increase the specificity of the measured sphingolipid species in endolysosomes and reduce the noise from other organelles and cellular compartments. Of note, the abnormal structure of lysosomes in *spp-10*-deficient worms shows striking similarities to those in *cpl-1*/cathepsin L-deficient worms (Zhang et al., 2023), the critical cathepsin required for phagolysosomal degradation of cell corpses in *C. elegans* (Xu et al., 2014). These results imply that glycosphingolipid accumulation impairs the degradative capacity of lysosomes, leading to cargo accumulation. This notion is confirmed by our observations that embryos defective in degrading glucosylceramides by low pH- and saposin C-dependent glucosylceramidases are not able to efficiently resolve cell corpses. Nonetheless, using our pH-sensitive GFP markers and CMBD assay we did not detect a defect in the initial phagolysosomal acidification and corpse membrane degradation. Instead, we noticed that corpse persistence in *spp-10*-deficient animals is mainly caused by a dysfunction in the formation of the detectable cargo-containing phagolysosomal vesicles. However, ARL-8, the GTPase mediating phagolysosome tubulation was recruited to *spp-10*-deficient phagolysosomes. further, we also found that SPP-10 is not required for normal localization of the amino acid transporter SLC-36.1. Similarly, protein degradation and amino acid transport out of phagolysosome are also not needed for ARL-8 recruitment but are essential for phagolysosome vesiculation (Fazeli et al., 2023b). Therefore, the formation of the cargo-containing phagolysosomal vesicles depends on protein and sphingolipid degradation downstream of ARL-8 recruitment. Thus, how sphingolipid accumulation leads to decreased formation of the cargo-containing phagolysosomal vesicles can only be speculated from our data. Intriguingly, dhCer species tend to primarily accumulate in ER. Considering that the same cellular machinery is involved in both organelle anterograde transport and phagolysosomal tubulation (Fazeli et al., 2023b; Pu et al., 2015), we hypothesize that contact sites between phagolysosome and other organelles including ER (Levin-Konigsberg et al., 2019) could prevent movement and allow tubulation. It remains to be determined whether such organelle contact sites could be disrupted by sphingolipid accumulation, and further investigations are needed to validate this hypothesis.

Altogether, our in *vivo* experiments provide valuable insights into the regulatory role played by sphingolipids during the final steps of phagolysosome resolution. Since prosaposin mutations cause severe forms of sphingolipidosis in humans and are associated with perinatal lethality in mice (Oya et al., 1998), studying the role of SPP-10 during corpse clearance in *C. elegans* provides valuable insight into disease progression associated with prosaposin deficiency.

CRediT authorship contribution statement

Gholamreza Fazeli: Writing – original draft, Visualization, Supervision, Funding acquisition, Formal analysis, Data curation, Conceptualization. **Veronika Perschin:** Methodology. **José Pedro Friedmann Angeli:** Supervision. **Burkhard Kleuser:** Supervision, Funding acquisition. **Christian Stigloher:** Supervision, Funding acquisition. **Rebecca Holzapfel:** Formal analysis, Data curation. **Agata Prell:** Formal analysis, Data curation. **Fabian Schumacher:** Writing – review & editing, Methodology, Formal analysis, Data curation.

Declaration of Competing Interest

The authors declare that they have no known competing financial interests or personal relationships that could have appeared to influence the work reported in this paper.

Data availability

Data will be made available on request.

Acknowledgements

The authors thank Daniela Bunsen, Claudia Gehrig-Höhn, Gabriele Königer, Sandhya Mani, and Susanne Scheu for technical assistance. We thank Chonglin Yang and Jie Zhang for providing worm strains. *spp-10 (ok1585)* strain was obtained from the Caenorhabditis Genetics Center (CGC), which is funded by NIH Office of Research Infrastructure Programs (P40 OD010440). Sibylle Schneider-Schaulies, Ann Wehman, and anonymous reviewers provided valuable comments on the manuscript. This work was funded by Deutsche Forschungsgemeinschaft (DFG) grants FA1046/3-1 to G.F., STI700/1–1 to C.S. and GRK2581 to B.K. and C.S. We also acknowledge the assistance of the Core Facility BioSupraMol, supported by the DFG. The JEOL JEM-2100 Transmission Electron Microscope is funded by the Deutsche Forschungsgemeinschaft (DFG – 218894163). The control values in Fig. 4N & O are re-used with permission from a published work (Fazeli et al., 2023b).

Author contributions

G.F. designed, performed, analyzed, and supervised experiments and wrote the manuscript with feedback from all authors. R.H. performed and analyzed experiments and together with V.P. prepared worms for sphingolipidomic analysis. A.P. and F.S. analyzed sphingolipids in worms by HPLC-MS/MS. J.P.F.A, B.K. and C.S. supervised experiments.

Appendix A. Supporting information

Supplementary data associated with this article can be found in the

online version at doi:10.1016/j.ejcb.2024.151411.

References

Alliance of Genome Resources, C., 2022. Harmonizing model organism data in the Alliance of Genome Resources. Genetics 220.

Barreda, D., Grinstein, S., Freeman, S.A., 2024. Target lysis by cholesterol extraction is a rate limiting step in the resolution of phagolysosomes. Eur. J. Cell Biol. 103, 151382.

Beer, K.B., Rivas-Castillo, J., Kuhn, K., Fazeli, G., Karmann, B., Nance, J.F., Stigloher, C., Wehman, A.M., 2018. Extracellular vesicle budding is inhibited by redundant regulators of TAT-5 flippase localization and phospholipid asymmetry. Proc. Natl. Acad. Sci. USA 115, E1127–E1136.

Brenner, S., 1974. The genetics of Caenorhabditis elegans. Genetics 77, 71–94.

Chitwood, D.J., Lusby, W.R., Thompson, M.J., Kochansky, J.P., Howarth, O.W., 1995. The glycosylceramides of the nematode Caenorhabditis elegans contain an unusual, branched-chain sphingoid base. Lipids 30, 567–573.

Consortium, Ce.D.M., 2012. large-scale screening for targeted knockouts in the Caenorhabditis elegans genome. G3 (Bethesda 2, 1415–1425.

Fazeli, G., Frondoni, J., Kolli, S., Wehman, A.M., 2023a. Visualizing phagocytic cargo in vivo from engulfment to resolution in caenorhabditis elegans. Methods Mol. Biol. 2692, 337–360.

Fazeli, G., Levin-Konigsberg, R., Bassik, M.C., Stigloher, C., Wehman, A.M., 2023b. A BORC-dependent molecular pathway for vesiculation of cell corpse phagolysosomes. Curr. Biol. 33, 607–621 e607.

Fazeli, G., Stetter, M., Lisack, J.N., Wehman, A.M., 2018. C. elegans Blastomeres Clear the Corpse of the Second Polar Body by LC3-Associated Phagocytosis. Cell Rep. 23, 2070–2082.

Fraser, A.G., Kamath, R.S., Zipperlen, P., Martinez-Campos, M., Sohrmann, M., Ahringer, J., 2000. Functional genomic analysis of C. elegans chromosome I by systematic RNA interference. Nature 408, 325–330.

Gan, Q., Wang, X., Zhang, Q., Yin, Q., Jian, Y., Liu, Y., Xuan, N., Li, J., Zhou, J., Liu, K., Jing, Y., Wang, X., Yang, C., 2019. The amino acid transporter SLC-36.1 cooperates with PtdIns3P 5-kinase to control phagocytic lysosome reformation. J. Cell Biol. 218, 2619–2637.

Green, R.A., Audhya, A., Pozniakovsky, A., Dammermann, A., Pemble, H., Monen, J., Portier, N., Hyman, A., Desai, A., Oegema, K., 2008. Expression and imaging of fluorescent proteins in the C-elegans gonad and early embryo. Method Cell Biol. 85 179 (-+).

Hanel, V., Pendleton, C., Witting, M., 2019. The sphingolipidome of the model organism Caenorhabditis elegans. Chem. Phys. Lipids 222, 15–22.

Henseler, M., Klein, A., Glombitza, G.J., Suziki, K., Sandhoff, K., 1996. Expression of the three alternative forms of the sphingolipid activator protein precursor in baby hamster kidney cells and functional assays in a cell culture system. J. Biol. Chem. 271, 8416–8423.

Hernandez-Tiedra, S., Fabrias, G., Davila, D., Salanueva, I.J., Casas, J., Montes, L.R., Anton, Z., Garcia-Taboada, E., Salazar-Roa, M., Lorente, M., Nylandsted, J., Armstrong, J., Lopez-Valero, I., McKee, C.S., Serrano-Puebla, A., Garcia-Lopez, R., Gonzalez-Martinez, J., Abad, J.L., Hanada, K., Boya, P., Goni, F., Guzman, M., Lovat, P., Jaattela, M., Alonso, A., Velasco, G., 2016. Dihydroceramide accumulation mediates cytotoxic autophagy of cancer cells via autolysosome destabilization. Autophagy 12, 2213–2229.

Kinoshita, M., Kyo, T., Matsumori, N., 2020. Assembly formation of minor dihydrosphingomyelin in sphingomyelin-rich ordered membrane domains. Sci. Rep. 10, 11794.

Levin-Konigsberg, R., Montano-Rendon, F., Keren-Kaplan, T., Li, R., Ego, B., Mylvaganam, S., DiCiccio, J.E., Trimble, W.S., Bassik, M.C., Bonifacino, J.S., Fairn, G.D., Grinstein, S., 2019. Phagolysosome resolution requires contacts with the endoplasmic reticulum and phosphatidylinositol-4-phosphate signalling. Nat. Cell Biol. 21, 1234–1247.

Li, Y., Chen, B., Zou, W., Wang, X., Wu, Y., Zhao, D., Sun, Y., Liu, Y., Chen, L., Miao, L., Yang, C., Wang, X., 2016. The lysosomal membrane protein SCAV-3 maintains lysosome integrity and adult longevity. J. Cell Biol. 215, 167–185.

Li, Y., Wang, X., Li, M., Yang, C., Wang, X., 2022. M05B5.4 (lysosomal phospholipase A2) promotes disintegration of autophagic vesicles to maintain C. elegans development. Autophagy 18, 595–607.

Link, J., Paouneskou, D., Velkova, M., Daryabeigi, A., Laos, T., Labella, S., Barroso, C., Pacheco Pinol, S., Montoya, A., Kramer, H., Woglar, A., Baudrimont, A., Markert, S. M., Stigloher, C., Martinez-Perez, E., Dammermann, A., Alsheimer, M., Zetka, M., Jantsch, V., 2018. Transient and partial nuclear lamina disruption promotes chromosome movement in early meiotic prophase. Dev. Cell 45, 212–225 e217.

Meyer, R.C., Giddens, M.M., Coleman, B.M., Hall, R.A., 2014. The protective role of prosaposin and its receptors in the nervous system. Brain Res. 1585, 1–12.

Morimoto, S., Yamamoto, Y., O'Brien, J.S., Kishimoto, Y., 1990. Distribution of saposin proteins (sphingolipid activator proteins) in lysosomal storage and other diseases. Proc. Natl. Acad. Sci. USA 87, 3493–3497.

Njume, F.N., Razzauti, A., Soler, M., Perschin, V., Fazeli, G., Bourez, A., Delporte, C., Ghogomu, S.M., Poelvoorde, P., Pichard, S., Birck, C., Poterszman, A., Souopgui, J., Van Antwerpen, P., Stigloher, C., Vanhamme, L., Laurent, P., 2022. A lipid transfer protein ensures nematode cuticular impermeability. iScience 25, 105357.

Oya, Y., Nakayasu, H., Fujita, N., Suzuki, K., Suzuki, K., 1998. Pathological study of mice with total deficiency of sphingolipid activator proteins (SAP knockout mice). Acta Neuropathol. 96, 29–40.

Pu, J., Schindler, C., Jia, R., Jarnik, M., Backlund, P., Bonifacino, J.S., 2015. BORC, a multisubunit complex that regulates lysosome positioning. Dev. Cell 33, 176–188.

Rorman, E.G., Scheinker, V., Grabowski, G.A., 1992. Structure and evolution of the human prosaposin chromosomal gene. Genomics 13, 312–318.

Schindelin, J., Arganda-Carreras, I., Frise, E., Kaynig, V., Longair, M., Pietzsch, T., Preibisch, S., Rueden, C., Saalfeld, S., Schmid, B., Tinevez, J.Y., White, D.J., Hartenstein, V., Eliceiri, K., Tomancak, P., Cardona, A., 2012. Fiji: an open-source platform for biological-image analysis. Nat. Methods 9, 676–682.

Scholz, J., Helmer, P.O., Nicolai, M.M., Bornhorst, J., Hayen, H., 2021. Profiling of sphingolipids in Caenorhabditis elegans by two-dimensional multiple heart-cut liquid chromatography – mass spectrometry. J. Chromatogr. A 1655, 462481.

Shayman, J.A., 2000. Sphingolipids. Kidney Int 58, 11–26.

Sun, Y., Li, M., Zhao, D., Li, X., Yang, C., Wang, X., 2020. Lysosome activity is modulated by multiple longevity pathways and is important for lifespan extension in C. elegans. Elife 9.

Tintori, S.C., Golden, P., Goldstein, B., 2020. Differential expression gene explorer (DrEdGE): a tool for generating interactive online visualizations of gene expression datasets. Bioinformatics 36, 2581–2583.

Wang, Y., Arnold, M.L., Smart, A.J., Wang, G., Androwski, R.J., Morera, A., Nguyen, K.C. Q., Schweinsberg, P.J., Bai, G., Cooper, J., Hall, D.H., Driscoll, M., Grant, B.D., 2023. Large vesicle extrusions from C. elegans neurons are consumed and stimulated by glial-like phagocytosis activity of the neighboring cell. Elife 12.

Weiler, S., Kishimoto, Y., O'Brien, J.S., Barranger, J.A., Tomich, J.M., 1995. Identification of the binding and activating sites of the sphingolipid activator protein, saposin C, with glucocerebrosidase. Protein Sci. 4, 756–764.

Xatse, M.A., Olsen, C.P., 2023. Defining the glucosylceramide population of C. elegans. Front. Physiol. 14, 1244158.

Xu, M., Liu, Y., Zhao, L., Gan, Q., Wang, X., Yang, C., 2014. The lysosomal cathepsin protease CPL-1 plays a leading role in phagosomal degradation of apoptotic cells in Caenorhabditis elegans. Mol. Biol. Cell 25, 2071–2083.

Zhang, Q., Li, Y., Jian, Y., Li, M., Wang, X., 2023. Lysosomal chloride transporter CLH-6 protects lysosome membrane integrity via cathepsin activation. J. Cell Biol. 222.